Comparing multilayer brain networks between groups

Introducing graph metrics and recommendations

Mandke, Kanad; Meier, Jil; Brookes, Matthew J.; O'Dea, Reuben D.; Van Mieghem, Piet; Stam, Cornelis J.; Hillebrand, Arjan; Tewarie, Prejaas

DOI
10.1016/j.neuroimage.2017.11.016

Publication date
2018

Document Version
Final published version

Published in
NeuroImage

Citation (APA)
Mandke, K., Meier, J., Brookes, M. J., O'Dea, R. D., Van Mieghem, P., Stam, C. J., Hillebrand, A., & Tewarie, P. (2018). Comparing multilayer brain networks between groups: Introducing graph metrics and recommendations. *NeuroImage*, *166*, 371-384. https://doi.org/10.1016/j.neuroimage.2017.11.016

NeuroImage 166 (2018) 371–384

Contents lists available at ScienceDirect

NeuroImage

journal homepage: www.elsevier.com/locate/neuroimage

Comparing multilayer brain networks between groups: Introducing graph metrics and recommendations

Kanad Mandke [a], Jil Meier [b,c], Matthew J. Brookes [d], Reuben D. O'Dea [e], Piet Van Mieghem [b], Cornelis J. Stam [f], Arjan Hillebrand [f], Prejaas Tewarie [d,*]

[a] School of Psychology, University of Nottingham, Nottingham, United Kingdom
[b] Delft University of Technology, Faculty of Electrical Engineering, Mathematics and Computer Science, Delft, The Netherlands
[c] Brain Center Rudolf Magnus, Department of Psychiatry, University Medical Center Utrecht, Utrecht, The Netherlands
[d] Sir Peter Mansfield Imaging Centre, School of Physics and Astronomy, University of Nottingham, Nottingham, United Kingdom
[e] School of Mathematical Sciences, University of Nottingham, Nottingham, United Kingdom
[f] Department of Clinical Neurophysiology and MEG Center, VU University Medical Center, Amsterdam, The Netherlands

ARTICLE INFO

Keywords:
Functional connectivity
Functional networks
Structural networks
Multilayer networks
Graph theory
Multi-modal imaging
Minimum spanning tree
Network comparison

ABSTRACT

There is an increasing awareness of the advantages of multi-modal neuroimaging. Networks obtained from different modalities are usually treated in isolation, which is however contradictory to accumulating evidence that these networks show non-trivial interdependencies. Even networks obtained from a single modality, such as frequency-band specific functional networks measured from magnetoencephalography (MEG) are often treated independently. Here, we discuss how a multilayer network framework allows for integration of multiple networks into a single network description and how graph metrics can be applied to quantify multilayer network organisation for group comparison. We analyse how well-known biases for single layer networks, such as effects of group differences in link density and/or average connectivity, influence multilayer networks, and we compare four schemes that aim to correct for such biases: the minimum spanning tree (MST), effective graph resistance cost minimisation, efficiency cost optimisation (ECO) and a normalisation scheme based on singular value decomposition (SVD). These schemes can be applied to the layers independently or to the multilayer network as a whole. For correction applied to whole multilayer networks, only the SVD showed sufficient bias correction. For correction applied to individual layers, three schemes (ECO, MST, SVD) could correct for biases. By using generative models as well as empirical MEG and functional magnetic resonance imaging (fMRI) data, we further demonstrated that all schemes were sensitive to identify network topology when the original networks were perturbed. In conclusion, uncorrected multilayer network analysis leads to biases. These biases may differ between centres and studies and could consequently lead to unreproducible results in a similar manner as for single layer networks. We therefore recommend using correction schemes prior to multilayer network analysis for group comparisons.

Introduction

The human brain is widely considered to be a complex network that can be studied by graph theoretical approaches. In such a description, nodes in the network correspond to anatomical regions and links typically refer to either structural or functional connections between those regions. Graph or network theory has been applied successfully to networks derived from a wide range of modalities, for example from functional magnetic resonance imaging (fMRI) (Bassett et al., 2008), magnetoencephalography (MEG) (Stam, 2014), electroencephalography (EEG) (Stam et al., 2007), diffusion tensor imaging (Iturria-Medina et al., 2008) and structural covariance (He et al., 2007). A key advantage of such an approach is that network theory enables characterisation of both the spatial organisation and the strength of the network connections (Bassett and Sporns, 2017). Various metrics, describing both nodal and global topological network characteristics, have been shown to provide useful quantitative descriptions of networks in order to reveal common pathways across diseases (Crossley et al., 2014), and to differentiate brain states during cognitive tasks (Braun et al., 2015; Micheloyannis et al., 2006). Despite its potential, the application of network theory to

* Corresponding author. Sir Peter Mansfield Imaging Centre, School of Physics and Astronomy, University of Nottingham, University Park, Nottingham, United Kingdom.
E-mail address: prejaas.tewarie@nottingham.ac.uk (P. Tewarie).

https://doi.org/10.1016/j.neuroimage.2017.11.016
Received 13 July 2017; Received in revised form 27 September 2017; Accepted 8 November 2017
Available online 11 November 2017

neuroimaging comes with several challenges, including: 1) How do we integrate information from networks across different neuro-imaging modalities from the same subject or group? 2) How do we compare networks between groups and experimental conditions in an unbiased way?

One of the advantages of network theory is the fact that it is modality invariant, i.e. the same network concepts can be applied to a wide range of data obtained from different modalities. However, networks obtained from different imaging modalities or from different frequency bands in the same subjects are usually treated in isolation using a single layer network approach. Yet, the field is increasingly acknowledging and elucidating how different types of networks are interrelated in a non-trivial way (Garcés et al., 2016). For instance, relationships between anatomical and functional networks are now established and often studied using computational models (Hlinka and Coombes, 2012). Moreover, recent studies suggest that functional networks are shaped by both monosynaptic and polysynaptic walks in the underlying structural network (Mehta-Pandejee et al., 2017; Meier et al., 2016a; Robinson, 2012). Likewise, covariance in cortical myeloarchitecture and in fMRI connectivity matrices can be explained by a nonlinear combination of MEG functional connectivity matrices (Hunt et al., 2016; Tewarie et al., 2016a). Importantly, for MEG and EEG, there is no reason why different frequency-specific networks would operate independently from one another (Tewarie et al., 2016b). All of this evidence advocates an integrative approach.

A generic framework that enables integration of information from different networks is the multilayer network approach. A multilayer network can be considered as a 'network of networks', which consists of individual network layers that are interconnected (Boccaletti et al., 2014; Van Mieghem, 2016). Thus, a given node in the multilayer network can be involved in different types of interactions. Multilayer networks can show non-trivial properties that are not merely the result of the sum of its layers (Kivelä et al., 2014; Nicosia et al., 2013; Sahneh et al., 2015). This approach has been applied effectively to several networks, such as social networks, transportation networks, and synthetic networks, demonstrating that empirical systems can be better understood when the influence of interacting networks are considered (De Domenico et al., 2013; Granell et al., 2013; Hernández et al., 2014). Multilayer network approaches have recently been introduced to the field of neuroscience (Brookes et al., 2016; Buldú and Porter, 2017; Crofts et al., 2016; De Domenico et al., 2016; Tewarie et al., 2016b; Yu et al., 2017), where different layers can correspond to different frequency-band specific networks or networks from different modalities. Lately, motif analysis of a multilayer network – where individual layers were made up of DTI and fMRI networks – was reported by (Battiston et al., 2017). Using the multilayer framework an MEG study extracted meaningful connectivity differences between patients with schizophrenia and healthy controls (Brookes et al., 2016). Another study demonstrated a non-trivial relationship between frequency-band specific MEG networks for intermediate regimes of coupling between layers (Tewarie et al., 2016b). Furthermore, a multilayer network approach has also been applied successfully to the connectome of the *C. elegans*, where gap junctions and neuromodulator layers were grouped into different layers (Bentley et al., 2016; Nicosia and Latora, 2015; De Domenico et al., 2015a).

Despite the obvious promise of these approaches, a key issue in the application of network theory is comparison between groups or conditions. Group comparison at the level of single layer networks can be challenging and biased by, for example, link density (van den Heuvel et al., 2017; Van Wijk et al., 2010). In other words, network measures depend on non-organisational properties of the network such as link density and average connectivity. As a result, it proves to be challenging to differentiate between alterations in the underlying ground truth that are due to an experimental manipulation or a disease process from those that are due to experimental choices. This can potentially inflate false positives or false negatives when comparing networks between groups, which we refer to here as the bias in group comparisons. There are no reasons why multilayer networks would be exempted from these biases. Given the recent studies on multilayer networks in different diseases (Brookes et al., 2016; De Domenico et al., 2016; Guillon et al., 2016; Yu et al., 2017), it is now crucial to elucidate how to compare multilayer networks between groups. For single layer networks, several sampling methods or schemes have been proposed to correct for the biases in estimates of topology that are due to link density or average functional connectivity for unweighted and weighted networks respectively (Van Wijk et al., 2010). Examples of schemes that result in an unweighted subnetwork are multi-threshold permutation correction (Drakesmith et al., 2015), the minimally connected component (MCC) (Jalili, 2016), balance between network efficiency and costs (ECO) (Fallani et al., 2017), a clustering optimization approach (Smith et al., 2015), the minimum spanning tree (MST) (Stam et al., 2014; Tewarie et al., 2015) and the union of shortest path trees (USPT) (Meier et al., 2015). The MCC is based on a thresholding scheme, where a threshold is chosen just above the level where the network gets disconnected into components. For ECO, a threshold is chosen that maximises the ratio between network efficiency and link density, whereas the MST corresponds to the tree (a loop-less subnetwork) with the minimal sum of all weights that spans the original network. The USPT corresponds to the union of shortest path trees rooted at each node in the graph. While these approaches to extract unweighted networks have demonstrated their value for single layer networks, it remains unclear whether these approaches generalise to multilayer networks. Approaches for weighted networks (Wang et al., 2010), such as normalising by the mean or range of connectivity values have so far been less promising (Van Wijk et al., 2010). In the current study, we introduce a simple approach to correct for differences in average connectivity between groups for weighted networks, based on singular value decomposition of the multilayer connectivity.

This paper is organised in the following way. We start with a theoretical section (1) on the basic mathematical concepts and metrics for multilayer networks, followed by a short description of generative models for multilayer networks. These generative models allow us to evaluate correction schemes for a given ground truth. We then show that multilayer network metrics are biased in a similar fashion as single layer network metrics (2), and evaluate existing and two new approaches as solutions to correct for biases in link density and average connectivity (3). We then demonstrate how sensitive a given approach is in revealing the true changes in network topology (4) since correction schemes are only useful if changes in the underlying topology can still be detected after the correction. We use synthetic networks based on generative models (e.g. a nonlinear preferential attachment model and a generative model for multilayer community networks) as ground truth, and we also apply the approaches to empirical MEG and fMRI data. Lastly, (5) we analyse how sensitive multilayer network metrics can detect group differences after application of the correction schemes.

Theory: multilayer network metrics

A multilayer network is the generic name for a complex network structure consisting of multiple networks. Nodes exist in a set of *layers* that correspond to different important features of the system under consideration, and links encompass connections between all possible combinations of nodes and layers. Specific widely-used special cases include: multi-weighted graphs, multilevel or multi-scale networks, multiplex networks, multi-relational networks or hyper-networks (Boccaletti et al., 2014). These different types of networks all fall under the multilayer network framework and can be obtained after applying specific constraints (Boccaletti et al., 2014). Here it is worth noting that multilayer network approach does not assume that the different layers are necessarily integrated. The multilayer framework leaves space to quantify the balance between distinctness and commonality among layers. There are several review papers for mathematically oriented readers on multilayer networks, please see (Boccaletti et al., 2014; De Domenico et al., 2013; Kivelä et al., 2014; Wang et al., 2013; Wider et al.,

2016). For a recent review on multilayer networks applied to neuro-imaging datasets see De Domenico (2017). Here, we focus on the aspects of multilayer networks that can be readily translated to neuro-imaging (Fig. 1).

A convenient representation of a multilayer network is its corresponding block adjacency matrix (Gomez et al., 2013; De Domenico et al., 2013; Van Mieghem, 2016). An f-layered multilayer network written in terms of a block adjacency matrix reads (Sahneh et al., 2015)

$$A = \begin{bmatrix} A_1 & H_{12} & \dots & H_{1f} \\ H_{21} & A_2 & & \vdots \\ \vdots & & \ddots & \\ H_{f1} & \dots & & A_f \end{bmatrix}, \tag{1}$$

where A_α corresponds to a symmetric, square adjacency matrix of a layer α, $1 \le \alpha \le f$, and H_{kl} to the coupling matrix between the layers k and l, where $1 \le k,\ l \le f$. A_α has the same dimensions for all layers ($n\,x\,n$). This means that every layer has the same number of nodes or brain regions. The between layer coupling matrix H_{kl} can take any form, e.g. fully connected or a diagonal matrix (e.g. $H_{kl} = cI$, where c is a constant and I the identity matrix). In view of the focus of recent theoretical studies, we concentrate on the following case where coupling matrices are special diagonal matrices ($H_{kl} = cI$), i.e. only introducing links between the same node (brain region) over all layers. In other words, we ignore cross-frequency coupling between distant areas for now, but note that the subsequent metrics can also be applied to the case of fully connected interlayer coupling.

The available topological metrics can be divided into: 1) distance class metrics 2) connection class metrics 3) spectral class metrics and 4) between layer dependency metrics (Hernández and Van Mieghem, 2011). Spectral class metrics correspond to properties related to the eigenvalues of the network of interest (Van Mieghem, 2010). Distance class metrics are metrics where the geodesic distance or hops play a crucial role, where a hop refers to a link along a path. Connection class metrics refer to cohesive subgroups of nodes or the connectedness of a single node in the network. Between layer dependency metrics correspond to metrics that quantify relationships between layers.

1) Distance class metrics

Similar to single layer networks, *characteristic path length*, S, and *global efficiency*, G, are measures of integration in the network and can be similarly defined as (Boccaletti et al., 2014)

$$S = \frac{1}{t(t-1)} \sum_{i,j,i \neq j} s_{ij} \tag{2a}$$

$$G = \frac{1}{t(t-1)} \sum_{i,j,i \neq j} \frac{1}{s_{ij}}, \tag{2b}$$

where the distances s_{ij} refer to the number of hops (links) that you must traverse to travel from one node i to another node j along the shortest path between them, and where $t = nf$. Distances can be obtained using Dijkstra's algorithm (Dijkstra, 1959). The global efficiency G can also be evaluated for a subnetwork consisting of only the neighbours of node i. This results in the metric *local efficiency* for every node, which is usually averaged across nodes in the neuroscience literature, yielding a single value per network (Rubinov and Sporns, 2010).

2) Connection class metrics

Several metrics exist in this class, such as metrics that quantify the "importance" or "hubness" in a network and other metrics that quantify clustering and community structure. A basic measure for "importance" for a given node i in multilayer networks is the *multilayer degree d.* This metric was introduced in its general form by (De Domenico et al., 2013), and for the special case of multiplex networks by (Battiston et al., 2014). We assume a node labelling such that node i belongs to the l-th block row in A (Van Mieghem, 2016)

$$\begin{aligned} d_i &= \sum_{l=1}^{f} (A_l u)_i + \sum_{b=1,b\neq l}^{f} \sum_{k=1;k\neq l}^{f} (H_{bk} u)_i \\ &= {}_l d_i + \sum_{b=1,b\neq l}^{f} \sum_{k=1;k\neq l}^{f} (H_{bk} u)_i, \end{aligned} \tag{3}$$

where ${}_l d_i$ is the degree of node i in the multilayer network layer l, $(H_{bk}u)_i$ are the inter-layer links from node i towards nodes at layer k, and u is the all-one vector. This multilayer degree metric is the extension of the degree from single layer networks. Extensions for *eigenvector centrality* to a multilayer framework also exist (Solá et al., 2013; Solé-Ribalta et al., 2014), as well as other more sophisticated measures, such as versatility of nodes and multilayer pagerank (De Domenico et al., 2015b; Halu et al.,

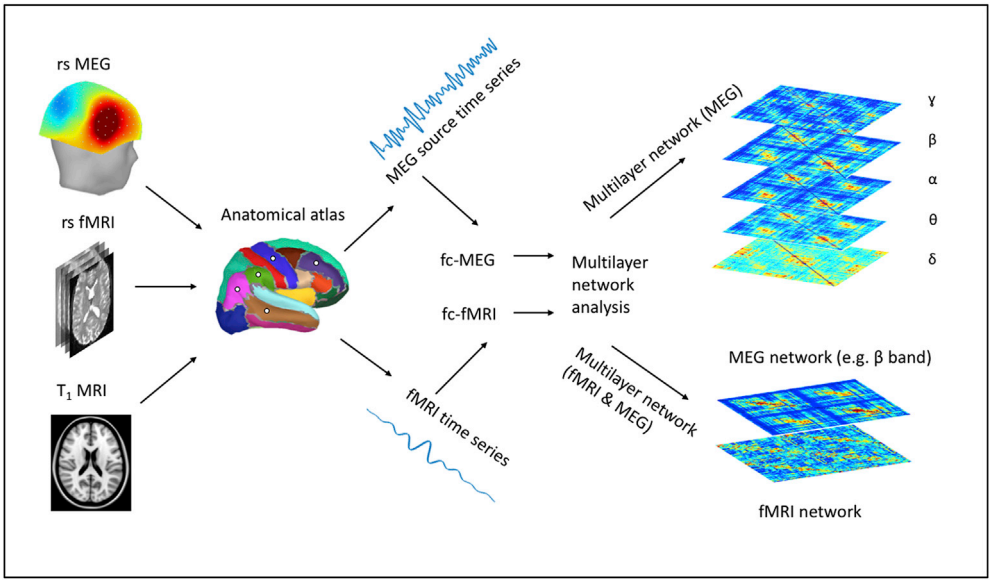

Fig. 1. A schematic of the analysis pipeline including construction of MEG specific multilayer network and a multimodal (fMRI-MEG) multilayer network. Note that we are treating a special case of multilayer networks: multilayer networks with one-to-one between layer coupling. rs: Resting state, fc: Functional connectivity.

2013). Multilayer pagerank is a metric based on biased random walks in a multilayer network. A very recent metric related to multilayer pagerank is *functional multilayer pagerank* (Iacovacci et al., 2016). This metric uses the concept of a multilink $\overrightarrow{m}_{ij} = (a^1_{ij}, a^2_{ij}, \ldots, a^f_{ij})$ and $\overrightarrow{m} = (m^1, m^2, \ldots, m^f)$, where a^l_{ij} refers to a connection between node i and j in layer l. The functional multilayer pagerank X_i depends on a tensor $\mathbf{z}$ with elements $z^{\overrightarrow{m}}$, and captures the probability $\tilde{\alpha}$ with which a random walker in the multilayer network jumps from one node i to a neighbour j (first term in Eq. (4a)) or to any other node in the multilayer network (second term in Eq. (4a))

$$X_i(\mathbf{z}) = \tilde{\alpha}\sum_{j=1}^{n} B_{ij}^{\overrightarrow{m}^{ij}} z^{\overrightarrow{m}^{ij}} \frac{1}{\kappa_j} X_j + \beta v_i. \tag{4a}$$

The first term contains the matrix B, which is called the multi-adjacency matrix

$$B_{ij}^{\overrightarrow{m}} = \prod_l^f \left[m_l a^l_{ij} + (1 - m_l)\left(1 - a^l_{ij}\right)\right], \tag{4b}$$

and reflects the neighbours of a node that are connected through a multilink. The probability that a random walker hops to a neighbour i is normalised by the following expression

$$\kappa_j = \sum_{j=1}^{n} B_{ij}^{\overrightarrow{m}^{ij}} z^{\overrightarrow{m}^{ij}} + \delta_{0,\sum_{j=1}^{n} B_{ij}^{\overrightarrow{m}^{ij}} z^{\overrightarrow{m}^{ij}}}, \tag{4c}$$

where $\delta_{b,c}$ corresponds to the Kronecker delta function. The product βv_i in Eq. (4a) describes a random jump to any other connected node in the network

$$\beta = \frac{1}{n}\sum_{j=1}^{n}\left[(1-\tilde{\alpha})\left(1 - \delta_{0,\sum_{j=1}^{n} B_{ij}^{\overrightarrow{m}^{ij}} z^{\overrightarrow{m}^{ij}}}\right) + \delta_{0,\sum_{j=1}^{n} B_{ij}^{\overrightarrow{m}^{ij}} z^{\overrightarrow{m}^{ij}}}\right] X_j \tag{4d}$$

$$v_i = \theta\left(\sum_{j=1}^{n} B_{ij}^{\overrightarrow{m}^{ij}} z^{\overrightarrow{m}^{ij}} + \sum_{j=1}^{n} B_{ji}^{\overrightarrow{m}^{ji}} z^{\overrightarrow{m}^{ij}}\right). \tag{4e}$$

Here, θ corresponds to the Heaviside function. By tuning $\mathbf{z}$, different versions of $X_i(\mathbf{z})$ can be obtained, however, in our case we are interested in the global ranking of the nodes, i.e. we are interested in $X_i^* = \max X_i(\mathbf{z})$. This maximum value can easily be found by expressing $\mathbf{z}$ in spherical coordinates (Iacovacci et al., 2016). The input to Eq. (4) can also be in the form of weighted adjacency matrices (Iacovacci et al., 2016).

The *clustering coefficient* on single layer networks has been generalised to multilayer networks. This metric captures the amount of segregation in the network in terms of triangles. In the multilayer version of the clustering coefficient C_i, a triangle can be formed by links in different layers (Battiston et al., 2014)

$$C_i = \frac{\sum_l \sum_{k\neq l} \sum_{j\neq i, j'\neq i} a^l_{ij} a^k_{jj'} a^l_{j'i}}{(f-1)\sum_{ll} d_i ({}_l d_i - 1)}, \tag{5}$$

where a^l_{ij} refers to a connection between node i and j in layer l. We note in passing that the multilayer clustering coefficient given by Eq. (5) can be extended to analyse (for example) structural–functional network relationships, and in particular their divergence under certain dynamical system conditions, in directed networks of relevance to neural systems (Crofts et al., 2016). Such ideas can be extended to weighted temporal (e.g. frequency band) networks.

Community detection algorithms have been widely applied to single layer brain networks. Community structure in fMRI networks has been shown to reveal similar clusters as resting-state networks obtained from independent component analysis (Crossley et al., 2013; Meunier et al., 2010). Details on multilayer community structure can be found in (Bassett et al., 2013; Mucha et al., 2010). Communities g_i are usually obtained after optimisation of a quality function, e.g. modularity (Newman, 2006), that quantifies within-community connections relative to connections between communities. The multilayer variant of modularity is expressed as (Bassett et al., 2013)

$$Q = \frac{1}{2u_{tot}} \sum_{ijlk} \left[\left(A_{l,ij} - \gamma_l \frac{{}_l d_i {}_l d_j}{2\sum_{il} d_i} \delta_{lk} \right) + \delta_{ij} H_{lk,j} \right] \delta_{g_{il}, g_{jk}}, \tag{6}$$

where u_{tot} corresponds to the total link weight in the network, γ_l to the resolution parameter, g_{il} stands for the community assignment of node i in layer l. Another way to extract communities is motif partitioning explained in (Benson et al., 2016), which has been applied to directed MEG networks in (Meier et al., 2016b; Märtens et al., 2017).

3) Spectral class metrics

Spectral metrics are based on the (eigen)spectrum of the block-matrix A or on the Laplacian Q of the multilayer network, obeying $Qx = \mu x$, where x and μ are an eigenvectors and eigenvalues (Van Mieghem, 2010), respectively, of Q, which is defined as

$$Q = \begin{bmatrix} \Delta_1 - A_1 & 0 & \ldots & 0 \\ 0 & \Delta_2 - A_2 & & \vdots \\ \vdots & & \ddots & 0 \\ 0 & \ldots & & \Delta_f - A_f \end{bmatrix} + \begin{bmatrix} \sum_l H_{1l} & -H_{12} & \ldots & -H_{1f} \\ -H_{21} & \sum_l H_{2l} & & \vdots \\ \vdots & & \ddots & \\ -H_{f1} & \ldots & & \sum_l H_{fl} \end{bmatrix}, \text{ with} \tag{7a}$$

$$\Delta_l = \mathrm{diag}({}_l d_1, {}_l d_2, \ldots, {}_l d_n), \tag{7b}$$

where ${}_l d_i$ $(1 \leq i \leq n)$ is the degree of node i in layer l (remember that every layer has n nodes). Let $\mu_1 \geq \mu_2 \geq \ldots \geq \mu_t$ be the ordered set of eigenvalues of Q, where $t = nf$. The second smallest Laplacian eigenvalue μ_{t-1} is called the *algebraic connectivity*. This metric is related to the time to synchronize phase oscillators in a network and also to the robustness of a network: a higher algebraic connectivity means a higher inter-twined subgraph structure, which makes it harder to fragment the graph (Hernández et al., 2014). A relatively novel way to capture topological information from the network is to analyse the pseudo-inverse $Q^\dagger$ of the Laplacian (Ellens et al., 2011; Van Mieghem et al., 2017). The *effective graph resistance* $\tilde{R}_G$ and the *zeta vector* can be obtained from this pseudo-inverse

$$\tilde{R}_G = t\,\mathrm{trace}\left(Q^\dagger\right) \tag{8a}$$

$$\zeta = \left(Q^\dagger_{11}, Q^\dagger_{22}, \ldots, Q^\dagger_{tt}\right) \tag{8b}$$

The effective graph resistance captures the overall transport ability: the lower $\tilde{R}_G$, the lower the resistance for flow in the network (Van Mieghem et al., 2017). The zeta vector captures the information of nodal spreading within the network. The *effective graph resistance* $\tilde{R}_G$ and the *zeta vector* are defined in both weighted and unweighted graphs.

4) Between layer dependency

In addition to well-known metrics for single layer networks, multilayer networks can also be characterised by their between-layer relationships, examples are: *entropy of multilayer degree*, *multilayer participation coefficient*, *conditional probability of finding a link in layer α given a link in layer α'*, *degree correlations* (Battiston et al., 2014; Wider et al., 2016). Entropy of multilayer degree follows the definition of

Shannon entropy with the probability replaced by ${}_{l}d_i/d_i$. Multilayer participation coefficient is related to the entropy and quantifies whether links of a given node i are uniformly distributed among layers (Battiston et al., 2014)

$$PC_i = \frac{f}{f-1}\left[1 - \sum_{l=1}^{f}\left(\frac{{}_{l}d_i}{d_i}\right)^2\right]. \quad (9)$$

Lastly, between layer degree correlations (DC) can be quantified by computing a Pearson correlation between the degree sequences of different layers (Battiston et al., 2014; Wang et al., 2014). These between layer dependency metrics allow one to capture whether individual layers act independently, in coherence with each other or in a regime between these two extremes, as recently demonstrated in (Tewarie et al., 2016b).

Theory: generative models for multilayer networks

Non-linear preferential attachment for multilayer networks

The first model we used is a nonlinear preferential attachment model (Nicosia et al., 2014). Here, the initial conditions are a small connected multilayer network consisting of n_0 nodes and with f layers. Then, for every time step during the reconstruction of the network, a node i is added to the multilayer network and connected to another node j with probability $\Pr_{i\to j}$ based on the multilayer degrees

$$\Pr_{i\to j} \propto f\left({}_{1}d_j, {}_{2}d_j, \ldots, {}_{f}d_j\right). \quad (10)$$

If we consider the case of a two-layered multilayer network (duplex, $f = 2$) we can choose the function f as

$$f\left({}_{1}d_j, {}_{2}d_j\right) = \left({}_{1}d_j\right)^{\alpha}\left({}_{2}d_j\right)^{\beta}. \quad (11)$$

By tuning α and β, different network configurations can be obtained, for example by tuning α or β from negative to positive we can construct layers with different correlations between their degrees (i.e. correlation between the degree sequence layer one vs degree sequence layer two). For the results section, we create a two-layer multilayer network consisting of 200 nodes and tune β to alter the interlayer dependency.

Synthetic multilayer community networks

The second generative model we used creates multilayer communities with tuneable between-layer dependency of these communities; details of the algorithm can be found in (Bazzi et al., 2016). In short, the algorithm consists of two sequential steps. First, a multilayer partition is constructed: Partitions in each layer are initialised independently and updated iteratively according to a user-defined interlayer dependency tensor. Then, a random multilayer network is generated using the previously defined multilayer partitioning. This is done using a generalisation of stochastic block models to multilayer networks (Karrer and Newman, 2011). A link is added in the multilayer network based on a probability that is proportional to the product of the partition, expected number of links between communities (user-defined), and the expected number of links within communities. In addition, the multilayer networks can be constructed with a fraction of random links. In the simulations presented in the results section the similarity of communities in the different layers is tuned by altering the interlayer dependency tensor.

Methods

Empirical MEG and fMRI networks

We make use of a previously published MEG/fMRI dataset (Tewarie et al., 2016a). A total of 15 participants (mean age 27.7 ± 6.5, 60% female) were used for analysis in this study. The study was approved by the University of Nottingham Medical School Ethics Committee, and all subjects gave written informed consent prior to participation.

MEG data were acquired using a 275 channel CTF MEG system (MISL, Coquitlam, Canada), at a sampling rate of 600 Hz and using a 150 Hz low pass anti-aliasing filter. Data were recorded during a task-free, eyes-open condition for 10 min with the subject in a supine position. Subjects were asked to fixate on a red cross throughout. The surface of the head was digitised using a 3D digitiser (Polhemus Inc., Vermont). Co-registration was achieved using surface matching of the digitised head shape to an equivalent head shape extracted from an anatomical magnetic resonance (MR) image. MEG data were inspected for artefacts and trials deemed to contain excessive interference were removed. Lead fields were based on equivalent current dipole models (grid spacing of 4 mm) and a multiple local sphere head model (Huang et al., 1999). Lead fields, the parcellated individual's cortex (automated anatomical atlas (AAL); (Gong et al., 2009; Tzourio-Mazoyer et al., 2002)), and sensor level MEG data were fed into a scalar beamforming approach (Hillebrand et al., 2012). Data covariance was computed within a 1–150 Hz frequency window and regularisation was applied to the data covariance matrix using the Tikhonov method with a regularisation parameter of 5%. Dipole orientation was determined using a non-linear search for optimal signal-to-noise-ratio. Beamformer timecourses were sign-flipped where necessary to account for the arbitrary polarity introduced by the beamformer source orientation estimation. Beamformer timecourses within a parcellated region were averaged using a Gaussian weighting function to obtain a representative timecourse for every region. This complete process resulted in 78 electrophysiological time courses, each representative of a separate cortical AAL region. Time courses were frequency filtered into five frequency bands: delta (1–4 Hz), theta (4–8 Hz), alpha (8–13 Hz), beta (13–30 Hz), gamma (30–48 Hz). This was followed by a multivariate orthogonalisation to correct for signal leakage (Colclough et al., 2015). Finally, a functional connectivity matrix was reconstructed by computing amplitude envelope correlations between leakage-corrected frequency-filtered timecourses (Brookes et al., 2011a).

MRI data were collected using a 7 T-MRI system (Philips Achieva) with a volume transmit and 32 channel receive head coil. The anatomical MR image (used for MEG source reconstruction as well as fMRI processing) was acquired using an MPRAGE sequence (1 mm isotropic resolution, TE = 3 ms, TR = 7 ms, flip angle = 8°). Bias fields were corrected using SPM8 and brain extraction for the MPRAGE was achieved using the Brain Extraction Tool (BET v2.1, FSL (FMRIB's Software Library, http://www.fmrib.ox.ac.uk/fsl)) (Smith et al., 2004). Resting-state fMRI data were acquired using a gradient-echo echo planar imaging sequence (TR = 2 s, TE = 25 ms, flip angle = 75°, voxel dimensions = 2 × 2 × 2 mm^3, 150 vol acquisitions). Participants were asked to keep their eyes open during the scan and to fixate on a cross presented on a back-projection screen and viewed via a mirror. Data were motion corrected using SPM8 (Ashburner et al., 1999). Subject-specific masks of grey matter, white matter, and cerebrospinal fluid (CSF) were obtained via automatic segmentation of the MPRAGE data (FAST v4.1 FSL (Smith, 2002)). The AAL atlas was used to parcellate the cortex into the same 78 regions of interest (ROIs) as used for the MEG data. The fMRI data were registered to the corresponding MPRAGE image, which was in turn registered to the MNI-152 template brain (FLIRT v5.5, FSL). Inverse transformations were calculated and used to register a grey matter mask and the AAL ROIs to the functional space for each subject. To maintain the consistency between the fMRI and MEG pipeline, a weighted average fMRI signal was computed to obtain a single signal for every ROI. We then regressed out average cerebrospinal fluid signal, average white matter signal, motion and 2nd order polynomials (i.e. low frequency trends) from each regional BOLD timecourse using a general linear model to remove non-neuronal signals. For each subject, pairwise Pearson correlation coefficients (absolute values) were computed between all possible 78 fMRI AAL signal pairs to obtain a connectivity matrix.

Schemes for the correction of network biases

For now, we consider a special case of multilayer networks, for which the interlayer coupling matrix $H_{KM} = cI$ (i.e. no cross-frequency coupling between different nodes). Here, c is a constant and I the identity matrix. Fig. 1 shows two possible ways to construct a multilayer network, one can either stack different frequency-band specific MEG networks as layers into a multilayer network or one can stack two networks from two different modalities, e.g. beta band MEG network (most similar to fMRI networks (Brookes et al., 2011a; Tewarie et al., 2016a)) and the fMRI network, into a multilayer network. There are of course other possible ways to construct multilayer networks (e.g. all MEG networks together with a structural network and fMRI network) that will be addressed in the discussion, but here we will restrict the analysis to the former two cases.

When treating a multilayer network based on different MEG connectivity matrices obtained with the same connectivity metric, the weights contain meaningful information. We therefore argue that a correction scheme should take the information regarding weight differences between the frequency bands into account. In the context of multilayer networks this is important with respect to layer dominance (Sahneh and Scoglio, 2014; Wang et al., 2014), i.e. one layer could be a stronger driver of multilayer network characteristics than other layers. Therefore, we propose a correction scheme that should be applied to the block-adjacency matrix (A), rather than a correction scheme that is applied to the adjacency matrices of every layer (A_α) separately. However, when treating a multilayer network based on different modalities, or based on different metrics using the same modality, the range of the link weights can be very different, and thus the differences in link weights for the different layers are artificial. Therefore, in such cases, we propose that a correction scheme should be applied to the individual layers (A_α) separately.

We employ four network correction schemes: the minimum spanning tree (MST), efficiency cost optimisation (ECO) and *two new methods*: effective graph resistance cost minimisation and network normalisation based on singular value decomposition (SVD). The first three approaches usually result in unweighted networks and correct for biases due to average degree or link density and aim to only include the backbone of the network. The SVD approach corrects for differences in average connectivity between groups and results in a weighted network (scaled version of the original network).

1) *MST:* the minimum spanning tree is a loop-less subnetwork that spans the original network using the minimum possible sum of link weights (Kruskal, 1956). The number of links in a tree is always equal to n-1 (or nf-1 for multilayer networks), and therefore no biases due to (differences in) link densities exist. After extracting the MST, link weights in this subnetwork are set to one. Furthermore, as long as the weight ordering is maintained, the MST is unaffected by manipulations of the original network. Strictly speaking, the MST gives a reduced topology rather than a correction, such as ECO. However, to remain consistent across all approaches, we also consider the MST as a correction scheme here.
2) *ECO:* efficiency cost optimisation is based on optimising the function $J = (G + Y)/\rho$, where G and Y are the global and local efficiency of the network (see Eq. (2)) and ρ the link density (fraction of links). It has been demonstrated analytically that the maximum for this function for different types of network topologies obeys $\rho \approx 3/(n-1)$, where n is the number of nodes (Fallani et al., 2017). In the case of multilayer networks this becomes $\rho \approx 3/(nf-1)$. Therefore, for all subsequent analyses, we only show results for this analytically obtained link density.
3) *Effective graph resistance cost minimisation:* Since there is evidence that large-scale communication in the brain is not merely shaped by efficiency, as inferred by a function of the shortest paths (Goñi et al., 2014; Meier et al., 2016a,b) and because of the risk of disconnected networks, we propose a different version of ECO. Instead of efficiency cost optimisation, we propose an effective graph resistance cost minimisation $F = \tilde{R}_G/\rho$. Since there is no analytical expression to determine the optimum value for F, we follow a numerical approach to find the minimum (this entails computing F for a range of link densities to determine the threshold that minimises F). This scheme is based on Eq. (8) and thus the correction scheme is applied to the block-adjacency matrix rather than to the individual layers separately.
4) *SVD normalisation:* For any matrix (block adjacency matrix A or adjacency matrix A_α) we can apply a singular value decomposition $A = U\Lambda V^T$, where U and V contain the left and right singular vectors and Λ the singular values of A. To correct for average connectivity/average link weight we can rescale Λ by the largest singular value λ_1. The rescaled matrix would thus become $\tilde{A} = U\left(\frac{10}{\lambda_1}\Lambda\right)V^T$. The multiplication by 10 is used to ensure that the range of values in $\tilde{A}$ is not too small and varies between 0 and 1. If A is a symmetric and square matrix, then a singular value decomposition returns the eigenvalues and eigenvectors. However, an eigenvalue decomposition can result in complex eigenvalues if A is non-symmetric and square (directed network) and therefore a singular value decomposition can be used to exclude potentially complex eigenvectors and eigenvalues.[1]

Results

Uncorrected multilayer networks are affected by average link weight or link density

To show the biases that can be introduced when a correction scheme is not applied, we first demonstrate how multilayer metrics vary as a function of link density (ρ) or average connectivity strength (<FC>: sum of weighted degrees) of an empirically based multilayer network. This multilayer network has two layers, corresponding to the group averaged alpha and beta band MEG networks. We applied different proportional thresholds, tuned the average functional connectivity strength, and subsequently computed four multilayer network metrics: degree correlation between layers (DC), mean functional multilayer pagerank (X), mean multilayer participation coefficient (PC) and multilayer modularity (Q).

Fig. 2A shows the different multilayer network metrics as a function of link density. Different thresholds for link density can non-trivially influence network metrics. Thus, choosing an arbitrary threshold for groups with different densities can artificially induce significant group differences in terms of multilayer network metrics. Fig. 2B shows the different multilayer network metrics as a function of average connectivity. Q is affected, since it is optimised in terms of the degrees, which scale with connectivity. Other metrics such as based on computing a correlation (DC) or ratios (PC) are naturally unaffected by differences in scale. However, to safely use all multilayer metrics on a weighted network, one would have to correct for average connectivity.

Applying correction schemes to multilayer networks as a whole

We apply four correction schemes to the block-adjacency matrix of the multilayer network in the previous section: MST, ECO, effective graph resistance cost minimisation and SVD normalisation. The multilayer network has two layers viz., alpha and beta band. First, MSTs are usually unaffected by a threshold, if a threshold applied to a network does not discard links that would be included in the MST, the MST computed on a thresholded network would be unaffected. However, this

[1] In general, the SVD is the eigenvalue decomposition of the Gram matrix, thus of A^TA (where A is an n x m matrix, and m can be different from n). In fact, for non-square matrices, the SVD was originally used (Golub and Van Loan, 2012).

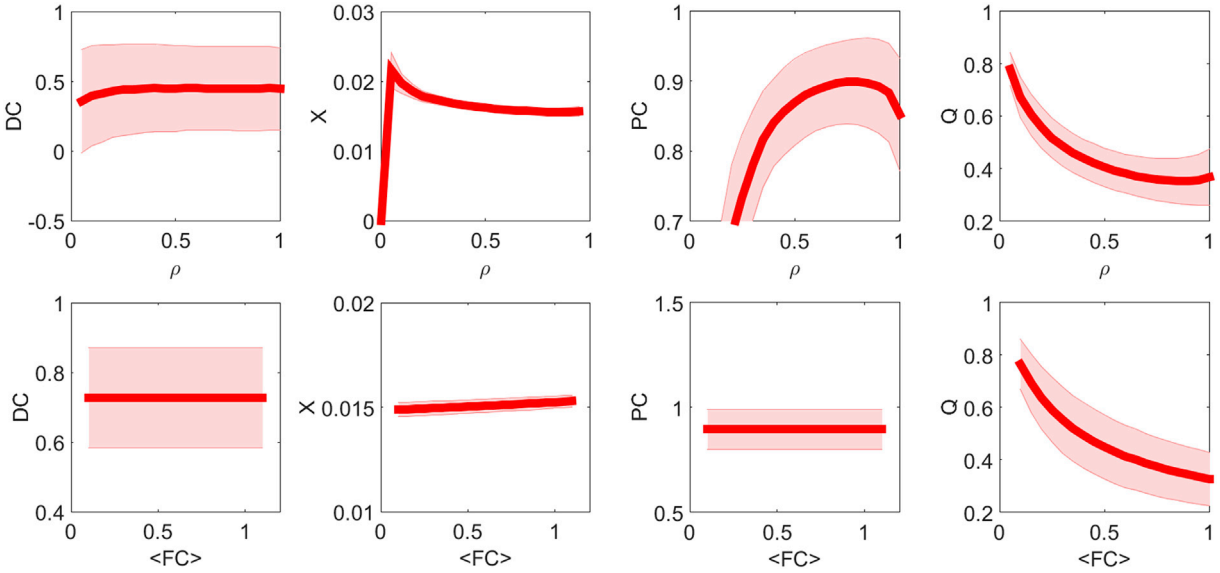

Fig. 2. Metrics are affected by changes in link density (A) and average connectivity (B). The plots show that tuning arbitrary link density (i.e. an arbitrary threshold), or the average connectivity, affects most of the metrics. However, this is not the case for DC and PC for changes in average connectivity. ρ = density, DC: degree correlation, X: functional multilayer page rank, PC: participation coefficient, Q: multilayer modularity, <FC>: average functional connectivity. The solid line and shaded areas show the mean and standard deviation across subjects, respectively.

stability is not observed in the case for MSTs computed on a multilayer network (Fig. 3A), where the MSTs computed for different link densities are not the same. The lack of uniqueness for the MST comes from the non-unique values of $H_{kl} = cI$ (c is chosen as the mean of the connections across all layers A_α). Furthermore, for most link densities, one of the individual layers can become disconnected (denoted by red dots in Fig. 3A). In Fig. 3B, we illustrate this, from layer one in this multilayer network, it can be inferred that not all nodes within a layer form a fully connected set in that layer, i.e. there are two connected components within the layer. Results for ECO are more stable compared to the MST. If the link density is above $\rho \approx 3/(nf-1)$, then the network with exactly this density is extracted. However, even after applying ECO, the resultant multilayer network can be disconnected either on the level of individual layers or the whole multilayer network (denoted by green dots in Fig. 3A). In Fig. 3D, we show effective graph resistance cost minimisation as a function of link density. Recall that the lower $\tilde{R}_G$ the lower the resistance for flow in the network. There is apparently no clear minimum for $\tilde{R}_G$, but $\tilde{R}_G$ reaches a plateau at around $\rho = 0.3$. Results for the SVD normalisation are shown in Fig. 3C. SVD normalisation leads to stable values for Q as a function of average functional connectivity (compare with Fig. 2B, right panel). The other metrics do not vary as a function of average connectivity either.

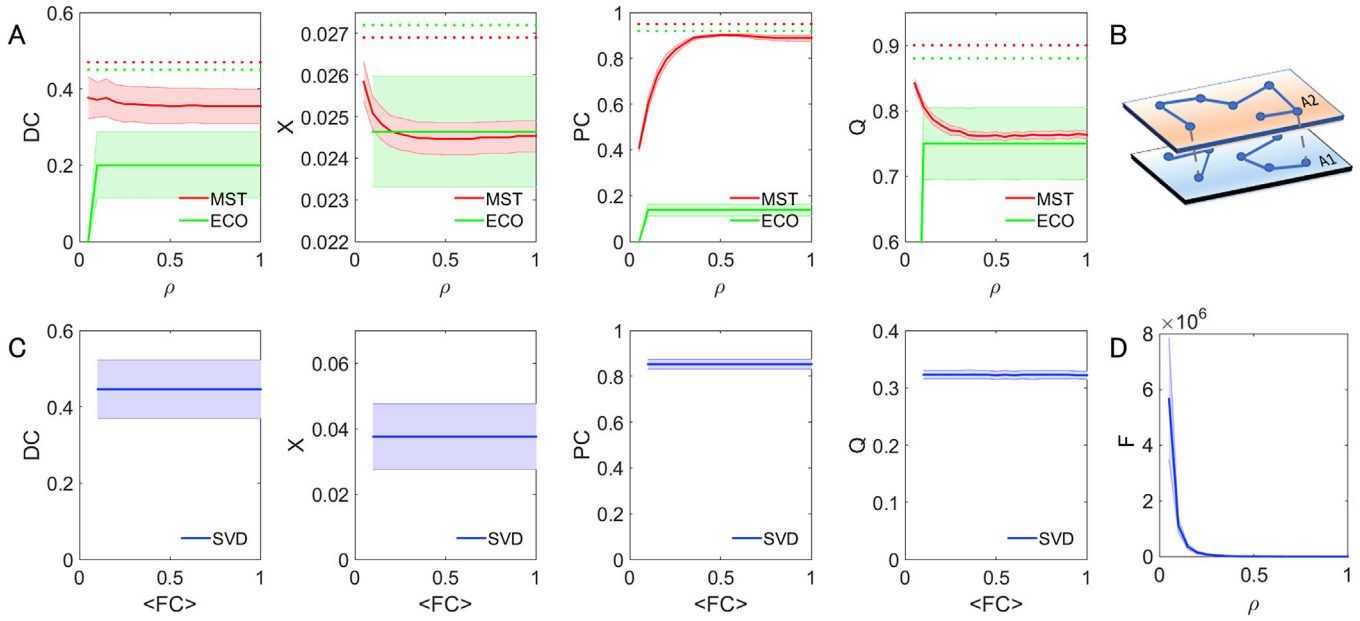

Fig. 3. The multilayer network made from participants' alpha and beta band networks. A) MST correction scheme on the multilayer network. This may result in a network that is connected but with disconnected individual layers, denoted by the multiple red dots and illustrated in (B). ECO correction scheme on the multilayer network (A). This can also lead to disconnected networks denoted by multiple green dots. C) SVD correction scheme on the whole multilayer network. D) Effective graph resistance cost minimisation. The solid line and shaded areas show the mean and standard deviation across subjects, respectively. ρ = density, <FC>: average functional connectivity, DC: degree correlation, X: functional multilayer page rank, PC: participation coefficient, Q: multilayer modularity, F: effective graph resistance cost minimisation.

Applying correction schemes to individual layers in multilayer networks

We consider the case of a two-layered multilayer network, consisting of layers obtained from a subject's beta band MEG network, and their fMRI network, i.e. from different modalities. Again, we show results based on individual subjects for which we illustrate the mean and standard deviation (Fig. 4). Instead of applying correction schemes to the block-adjacency matrix, we apply the four correction schemes to the individual layers. Fig. 4A shows the MST (red) and the ECO based networks (green) for different link densities. The stability of multilayer network metrics after applying the correction schemes MST and ECO. Unlike for the correction to the whole block-adjacency matrix (Fig. 3A), the MST does not depend on the non-unique values of H_{KM}, and therefore the weights for calculating the MST are unique, which results in stable and unique MSTs. Note though that non-unique link weights within individual layers can lead to non-unique MSTs. The SVD normalisation again results in a correction for biases in average connectivity (Fig. 4B). For effective graph resistance cost minimisation, a plateau is reached for layer 1 (beta band MEG) for $\rho = 0.6$ and $\rho = 0.25$ for layer 2 (fMRI network). Again, no local minimum is observed in this domain for ρ. Lastly, the choice of correction scheme might affect the ability to detect group differences (i.e. larger variability might hide genuine group differences). The sensitivity to detect changes in network topology is therefore assessed in the next paragraphs.

Nodal community assignment in multilayer networks after applying correction schemes

The SVD correction scheme applied to the whole multilayer network and the SVD, MST and ECO applied to individual layers are able to adequately correct for differences in average connectivity or link density. However, the magnitude of Q for instance gets altered after applying correction schemes. It is therefore important to assess to what extent the underlying communities change after applying a correction schemes. In Fig. 5 we show the community assignment for every node on a brain plot for the original multilayer network (empirical alpha and beta band network) and the community assignment for a node after applying the correction schemes. A sensorimotor network (green) and a visual network (red) can clearly be identified, which are dominant patterns in the beta and alpha band respectively. It can be observed that only SVD is able to correctly identify the original networks. Lastly, one should be cautious with community assignment in a tree (MST) with conventional methods, i.e. there will never be more links within a module than between modules. An alternative is the hierarchical clustering method evaluated in (Yu et al., 2015). The latter was not applied in the current work to keep consistency for all correction schemes.

Sensitivity to genuine alterations in multilayer network organisation – correction applied to multilayer networks as a whole

Given the ability of some of the schemes to correct for non-topological biases, we now analyse the sensitivity of network metrics to changes in network topology after applying correction to the block-adjacency matrix. Sensitivity in this context is referred as the ability of multilayer graph metrics to detect changes in the ground truth. Analysis is only performed for the SVD normalisation, since results from the previous paragraph showed that MSTs computed on the entire multilayer network resulted in non-unique MSTs, the ECO approach resulted in disconnected networks, and effective graph resistance cost minimisation did not yield a unique global minimum that could serve as a plausible link density. First, we use the multilayer community model and the nonlinear preferential attachment model to construct two layered synthetic multilayer networks with a known ground truth. In each model, we tune between-layer dependencies, which influences the similarity in communities or degree sequences across the two layers, respectively. This is done by altering the inter-layer dependency tensor for the multilayer community model or by tuning β for the nonlinear preferential attachment model. Fig. 6A shows the behaviour of the modularity Q as a function of between layer dependency in the original multilayer network and in the SVD corrected version. By applying SVD normalisation, there is a reduction in sensitivity to similarity in communities between layers and an overestimation of Q (Q from the corrected network is higher than from the ground truth). Although, the Q values based on SVD normalisation still correlate strongly with the underlying ground truth (Fig. 6C).

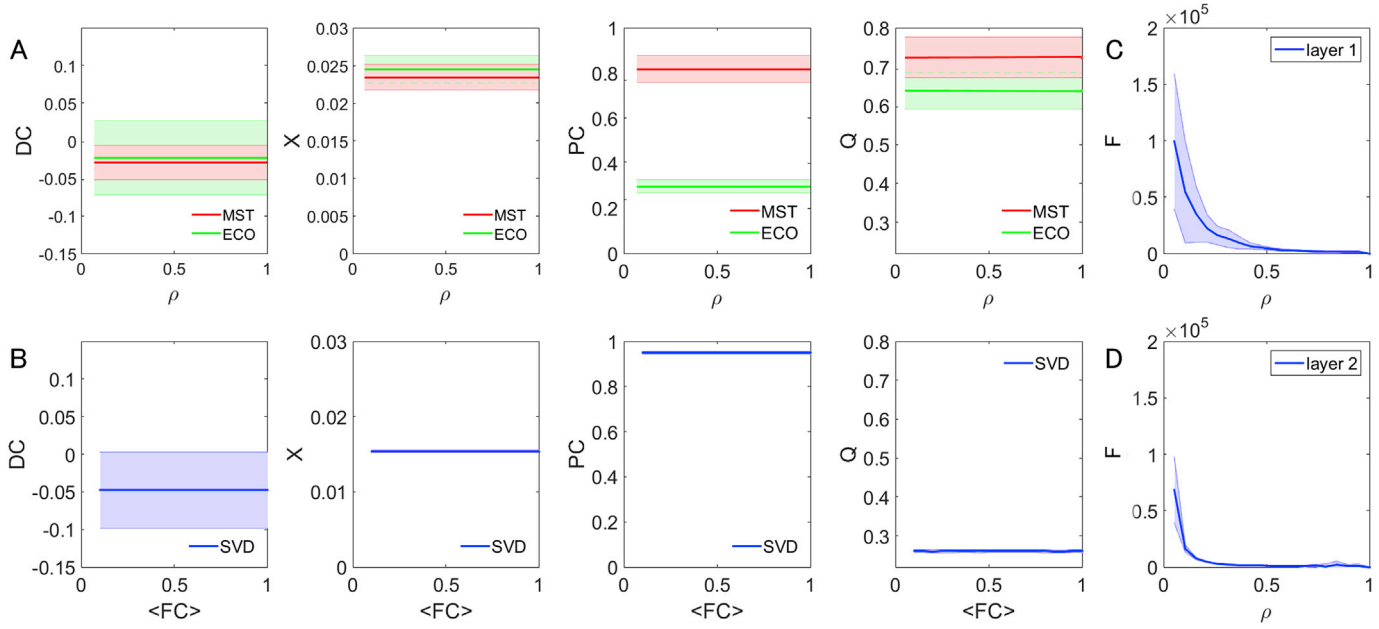

Fig. 4. The multilayer network made from participants' beta band MEG and fMRI networks. A) MST and ECO correction schemes applied to the individual layers. B) SVD correction scheme applied to individual layers. CD) Effective graph resistance cost minimisation in the two layers. The solid line and shaded areas show the mean and standard deviation across subjects, respectively. ρ = density, <FC>: functional connectivity, DC: degree correlation, X: functional multilayer page rank, PC: participation coefficient, Q: community structure, F: effective graph resistance cost minimisation.

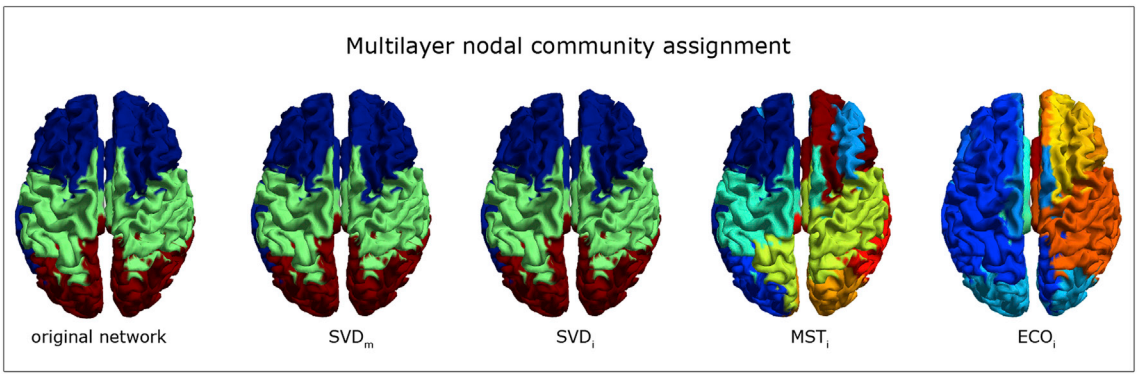

Fig. 5. Community assignment of multilayer networks (alpha and beta band) after applying correction schemes. Nodes that have the same colour belong to the same community (shown for the first layer here). On the outmost left, the original community assignment for every node is shown and further to the right the assignment after applying correction schemes is visualized. Only SVD applied on the whole multilayer (SVD_m) and on the individual layers (SVD_i) are able to correctly identify the communities. ECO and MST applied to the individual layers distort community assignments of nodes.

Fig. 6B shows the degree correlation as a function of between layer dependencies. The SVD normalisation clearly follows the degree correlation of the underlying multilayer network. This can also be observed from the strong correlation between ground truth and degree correlation after SVD normalisation (Fig. 6D).

In addition to applying the correction scheme to synthetic data, we now use empirical MEG data to analyse the sensitivity of SVD normalisation to underlying changes in network organisation. The multilayer networks are again two layered networks with a subject's alpha and beta band networks as layers. We alter a subject's given network organisation in these empirical multilayer networks by adopting a rewiring scheme. For a given probability *P*, we randomly swap matrix elements within the layers without preserving the degree distribution. Fig. 6E shows how multilayer network community structure alters as a function of increasing rewiring probability for original multilayer networks and SVD corrected multilayer networks. The SVD obtained Q values correlate strongly with the Q values obtained from the original multilayer networks (Fig. 6G). The same is also observed for degree correlation, i.e. SVD corrected DC values correlate strongly with the original DC values (Fig. 6F, H).

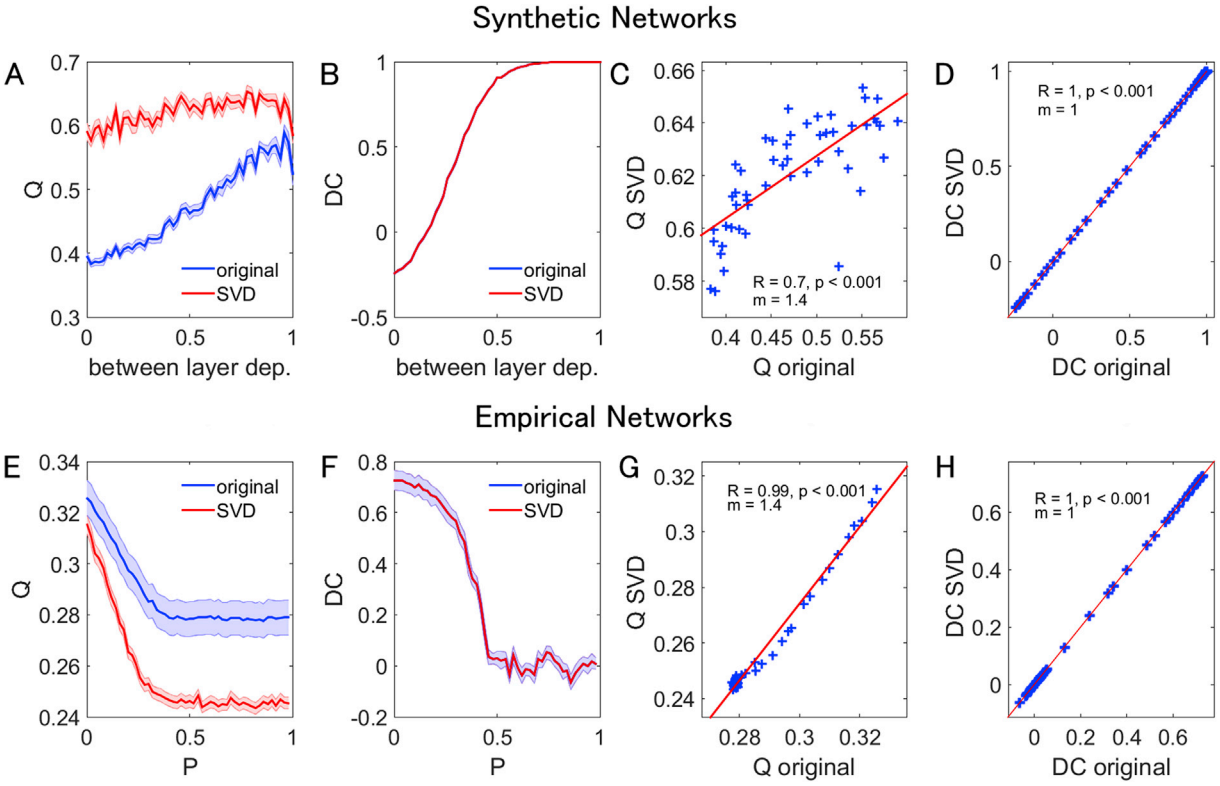

Fig. 6. 1st row: sensitivity of network metrics to changes in network organisation of the (synthetic) multilayer networks before and after applying SVD. A) Synthetic modular multilayer networks: modularity (Q) as a function of between layer dependency on the ground truth (blue) and SVD corrected networks (red). B) Synthetic scale free multilayer networks: degree correlation (DC) as a function of between layer dependency on the ground truth (blue) and SVD corrected networks (red) (both are completely overlapping). C) Correlation between Q as obtained before and after SVD. D) Correlation between DC as obtained before and after SVD. 2nd row: sensitivity of network metrics to changes in network organisation of the (empirical) multilayer networks. E) Q as a function of rewiring probability (P) for original networks (blue) and SVD corrected networks (red). F) Degree correlation (DC) as a function of rewiring probability for original networks (left) and SVD corrected networks. G) Correlation between Q as obtained before and after SVD. H) Correlation between DC as obtained before and after SVD. The shaded areas in A and B show the mean and standard deviation across realisations (A, B) or subjects (E, F).

Sensitivity to genuine alterations in multilayer network organisation – correction applied to individual layers in multilayer networks

We now demonstrate the sensitivity of network metrics after correction has been applied to individual layers. For both generative models, we again tune interlayer dependency and analyse how sensitive the correction schemes are (MST, ECO, SVD normalisation). Effective graph resistance cost minimisation was not used any further since previous analysis (see Fig. 4CD) did not yield in plausible link density for *F*. Fig. 7A shows Q for the synthetic modular multilayer networks for both the ground truth and correction schemes. All correction schemes overestimate Q and this overestimation is especially the case for MST and ECO. Fig. 7C shows the correlation between Q obtained from the ground truth and the correction schemes, and the slopes for MST and ECO are smaller than for SVD, indicating that the latter correction scheme is more sensitive to changes in community structure of the underlying ground truth. Fig. 7B and D shows the degree correlation between layers as a function of between-layer dependency and the correlation between ground truth DC and DC obtained after application of the correction schemes. DC values for all schemes are almost exactly preserved after applying the correction schemes and correlate strongly to the underlying ground truth.

In addition to synthetic networks, we again use empirical data to analyse the sensitivity of network metrics changes in network organisation after correction using SVD normalisation, MST and ECO. Again, corrections were applied to individual layers. The multilayer networks consist of subjects' beta band MEG network and their fMRI network. We follow a rewiring scheme equivalent to that described in the previous section. Fig. 7E, G shows Q as a function of rewiring probability for the original multilayer network and Q values obtained after application of the correction schemes. A good linear fit is obtained between the modularity values for the original network and the values obtained after application of the different correction schemes (Fig. 7G), although the range of values for Q obtained after correction is very different compared to those obtained for the original empirical multilayer network. Since MST and ECO include less weak connections, less influence of noisy connections is potentially driving up Q. Again, for DC, we clearly see that correction schemes follow the original DC values (Fig. 7F, H).

Sensitivity for identification of group differences

Figs. 6ACEG and 7ACEG indicate how sensitive multilayer network metrics are to changes in network topology after applying correction schemes. However, such curves are usually not obtainable in empirical studies where the interest lies in the detection of group differences. We therefore simulate two different distributions of Qs, based on the generative model for multilayer community networks, and analyse if these differences in distributions can be detected after applying correction schemes. Analysis for DC is omitted since Figs. 6BDFH and 7BDFH show that DC values are almost exactly preserved after applying correction schemes. We simulate two conditions: I) two sets of multilayer networks with a between layer dependency of 0.6 and 10% and 14% random links, respectively; II) two sets with 10% random links, but with a between-layer dependency of 0.4 and 0.7, respectively. Each set consists of 200 multilayer network realisations. Fig. 8 shows two sets of Qs for the original networks and for the networks obtained after applying the correction schemes: Q after correction on the whole multilayer SVD_m, Q after correction on individual layers SVD_i, and Q after MST and ECO applied to individual layers. All metrics computed after correction schemes can detect group differences for condition I and II (Fig. 8A, B).

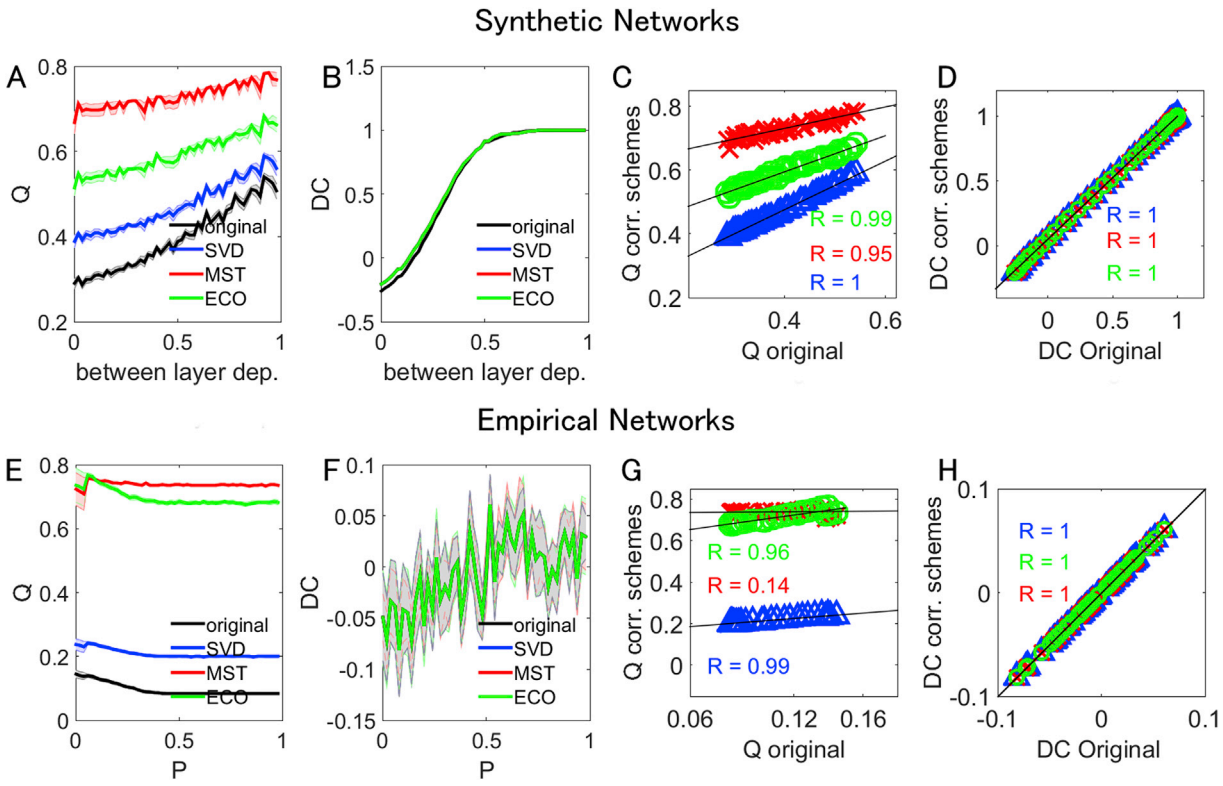

Fig. 7. Sensitivity of metrics to changes in network organisation of the (synthetic) multilayer networks. Synthetic modular multilayer networks: Community (Q) as a function of between layer dependency on the ground truth and on corrected networks (A). Synthetic scale free multilayer networks: degree correlation (DC) as a function of between layer dependency on the ground truth and corrected networks (B). Correlation between modularity as obtained before and after correction schemes (C). Correlation DC as obtained before and after correction schemes (D). Sensitivity of solutions to changes in network organisation of the (empirical) multilayer networks. Empirical multilayer networks: Community (Q) as a function of rewiring probability (P) for original networks (black) and corrected networks (E). Empirical multilayer networks: degree correlation (DC) as a function of rewiring probability (P) for original networks (black) and corrected networks (F). Correlation between modularity as obtained before and after correction schemes (G). Correlation of DC as obtained before and after correction schemes (H). The shaded areas show the mean and standard deviation across realisations (A–B) or subjects (E–F).

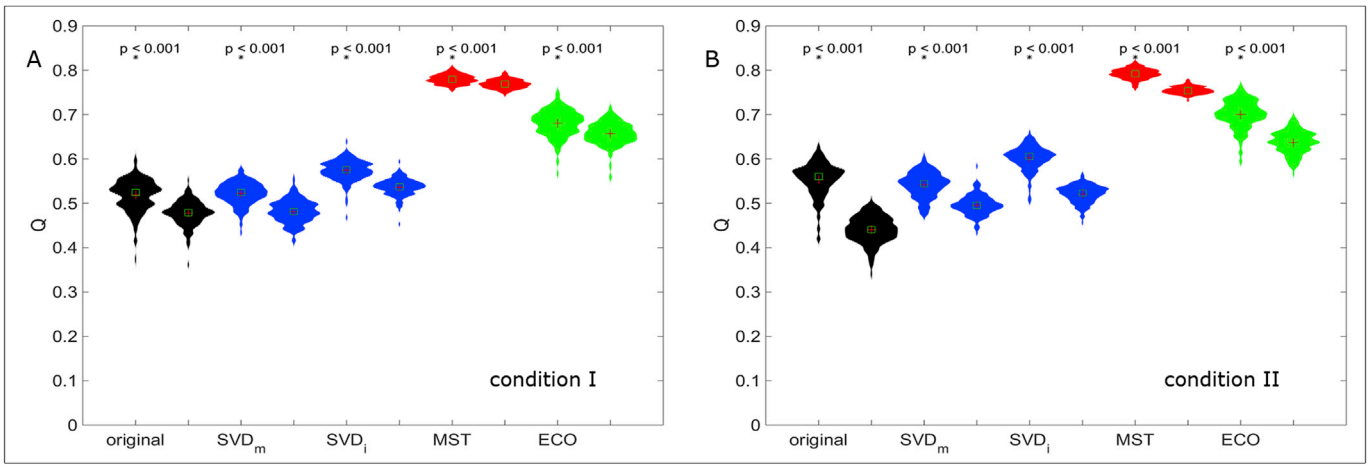

Fig. 8. Distributions of Q for two groups. Group differences of multilayer network community structure for the ground truth (black), SVD approach (blue), MST (red), and ECO (green). Both whole multilayer network correction as well as individual layer correction are applied for SVD, the former is denoted as SVD_m and the latter as SVD_i. A and B refer to two different conditions: I) different number of random links for the two sets; II) different between layer dependency for the two sets.

However, note that most of the correction schemes change the shape of the original distributions (black). Furthermore, note that the two distributions for the SVD_m groups overlap more than the groups for the other correction schemes, which is in line with the smaller slope in Fig. 6A (red one) compared to the slopes in Fig. 7C.

Discussion

Multilayer network framework allows for integration of information from different modalities in a unified network, where each layer of the network corresponds to network obtained from different neuro-imaging modalities or in the context of M/EEG data, to each frequency band (Brookes et al., 2016; Tewarie et al., 2016b). Firstly, we evaluated four different correction schemes to correct for biases in multilayer network metrics that are due to differences in link density and average connectivity. We examined two cases: 1) multilayer networks based on frequency band specific MEG networks; 2) multilayer networks based on networks from different modalities (fMRI and beta band MEG). For case one: only the SVD normalisation sufficiently corrected for biases due to average connectivity, while other schemes could not correct for biases sufficiently. For case 2: our results showed that the correction schemes MST, ECO and SVD normalisation all corrected successfully for biases due to link density or average connectivity, while effective graph resistance cost minimisation did not result in plausible link densities. Second, we evaluated the sensitivity of these approaches to detect changes in network organisation of the underlying ground truth, after these correction schemes were applied. Results for case one showed that metrics computed after SVD normalisation were indeed sensitive in identifying alterations in underlying network organisation, while for case two, metrics computed after MST, ECO and SVD were all shown to be sensitive.

For corrections applied to the entire multilayer networks, only the SVD approach resulted in appropriate correction for non-topological biases since this approach corrected for differences in average connectivity of the different layers. This approach can be applied to complete weighted multilayer networks where different link weight distributions in different layers contain relevant information. For example, in several cognitive experiments, gamma band connections can be more dominant and relevant in relation to the cognitive demand than other frequency bands (Doesburg et al., 2008; Fries, 2009; Senkowski and Gallinat, 2015). Thus, preserving the dominance of the gamma band in such conditions would be in line with the relevant task modulations. However, this is not strictly limited to modulations in gamma band. For example, a working memory task may lead to changes in theta band (Jensen and Tesche, 2002). Therefore, it is important that the representation of dominant frequency band (or layer) is preserved even at the network analysis stage. It is worth noting that in conditions where there is a dominant frequency band, individual layer normalisation would likely lead to equally important frequency bands in a multilayer network, this would in turn smear the underlying effects of interest.

The three other correction schemes, applied to the multilayer networks as a whole, did not result in sufficient correction. The ECO correction scheme sometimes led to disconnected multilayer networks, which limits its applicability. The effective graph resistance cost approach led to a plateau of values rather than a local minimum, indicating that not a single link density can be selected as a threshold that maximises flow in the network. The MST applied to the entire multilayer network did not yield unique MSTs. Reconstruction of the MST entirely depends on the ordering of the link weights and non-unique matrix elements can lead to arbitrary ordering. In our case, we encountered non-unique values as the interlayer coupling matrix was based on the identity matrix. The higher the threshold, the higher the probability of non-unique values, which leads to the scaling of MST metrics with link density in Fig. 3A. In addition, the number of matrix elements in the block-matrix is equal to $(nf)^2$, thus the more layers, the larger the probability to encounter matrix elements with the same values. This problem can be solved by estimation of, for example, one-to-one cross-frequency coupling. Another option is to place random numbers on the diagonal of the interlayer coupling matrices; however, this does not solve the problem, since different initialisations will result in different non-unique MSTs. Lastly, whilst the MST of the whole multilayer network is by definition connected, its application can lead to individual layers with unconnected components. Empirically, this means that the brain within a frequency band of interest, e.g. alpha band, does not form a connected network. Given the vast literature on electrophysiological networks (Bastos and Schoffelen, 2015; Larson-Prior et al., 2013), this seems biologically implausible.

Unlike for the whole multilayer network, most correction schemes applied to individual layers were successful in correcting for differences in average connectivity or link density. This approach is sensible when the natural range of link weights in different layers is distinct, due to, for example, usage of different connectivity metrics or the extraction of networks from different modalities. Only the effective graph resistance cost approach applied to individual layers was not successful, as this led, again, to a plateau of values rather than a local minimum, i.e. no single link density could be selected as a threshold to maximise flow in the network. In addition, the link density at which the plateau was reached was a lot higher than the density of connectomes obtained after ECO (see

(Fallani et al., 2017)). This indicates the arbitrary nature of this type of corrections.

Metrics computed on the whole multilayer network after SVD correction correlated strongly to network topology of the underlying ground truth. This was more evident for empirical multilayer networks than synthetic multilayer networks (compare Fig. 6A and E): although metrics computed on SVD corrected synthetic networks followed the direction of change of the underlying topology, there was a decrease in sensitivity to changes in topology, i.e. the red curve (SVD) has a less steep increase than the blue curve (original network) in Fig. 5A. The reason for this decrease in sensitivity in synthetic networks is that the SVD approach applied to a sparse network (as was the case for the synthetic networks) can lead to an artificially small noise floor for links that were initially zero in the original network. This is, however, not the case for the fully connected networks found empirically, and as can also be seen from Fig. 5EG, where metrics computed on SVD corrected empirical networks correlated strongly to metrics computed on the original networks. Metrics computed on multilayer networks after individual layer correction all correlated strongly to network topology of the underlying ground truth. This maintenance of sensitivity also resulted in the sensitivity to detect group differences.

Some methodological choices and findings warrant some further discussion.

1. The drawback of the SVD correction scheme is that it does not filter potentially noisy connections. It leads to a rescaling that adequately corrects for differences in average connectivity, but does not lead to sparse networks like the MST or ECO. There are methods in image processing to perform noise reductions for matrices based on SVD (De Moor, 1993); however, non-smoothness in a weighted adjacency matrix can be genuine and does not necessarily imply noise. If one is interested in obtaining a sparse multilayer network and when correction to the entire multilayer network is required, one potential option to solve the problem of noisy connections could be a sequential correction: first a link weight normalisation based on SVD on the whole multilayer network followed by extracting an MST or applying ECO on individual layers with preservation of the link weights.
2. If a weighted adjacency matrix is symmetric, then an SVD approach is equivalent to an eigenvalue-decomposition approach. This would mean that we are normalising the eigenvalues of the weighted adjacency matrix by the largest eigenvalue. The advantage of SVD, however, becomes apparent when directed networks are treated, since these networks correspond to non-symmetric matrices for which an eigenvalue-decomposition approach could lead to complex eigenvalues.
3. Here we treated multilayer networks based on either different MEG frequency-band specific networks obtained using the same connectivity metric or a two-layered network consisting of MEG and fMRI networks. However, the flexibility of the multilayer network also allows the construction of networks of various kinds. Correction of such networks can be performed by combining the currently explored methods. Examples of different flavours of multilayer networks can be: a number of frequency-band specific MEG networks obtained with a connectivity metric, stacked with a number of MEG networks obtained with a different connectivity metric or a multilayer network consisting of different frequency-band specific MEG networks together with a fMRI and structural network. In these cases, one could apply correction schemes to specific subsets before joining the sets together. For example, apply an SVD to all layers obtained with a single metric as a whole, apply SVD on the individual fMRI network layer, and apply SVD on an individual structural network layer.
4. Fourth, in the current setting and for simplicity, we evaluated one-to-one coupling between layers, but there is no methodological hurdle to apply the explored approaches to multilayer networks with richer and more realistic between-layer coupling matrices.
5. Fig. 7F shows the correlation between the degrees of MEG beta band networks and fMRI network from individual subjects. These values are very low, but can be explained by the fact that similarity between fMRI and MEG networks are much more apparent when averaging over subjects (Brookes et al., 2011b; Tewarie et al., 2016a).
6. Note that all multilayer network results from empirical data will be influenced by methodological choices prior to calculation of multilayer network metrics such as the connectivity metric of choice (Colclough et al., 2016), source localization method and forward model for MEG (Hincapié et al., 2017) and the parcellation scheme (Proix et al., 2016; Lord et al., 2016).
7. It is important to realise that any correction scheme or sampling method comes with the risk of leaving out genuine connections. Filtering can therefore influence group differences after applying correction schemes. In addition, applying correction schemes can leave the relative response to a perturbation intact, but the magnitude of the network metrics may change.
8. Lastly, although a fair number of network metrics were enumerated and evaluated, our choice of metrics could have influenced the stability of the results. It is important to stress that the proposed correction schemes have been evaluated within the limits of the current datasets, pipelines and network metrics. The evaluation of other network metrics and approaches in the context of other generative models and connectivity metrics also deserves further attention in future work.

We used a specific set of four correction schemes in the current study, despite the presence of more proposals in the literature. The reason to restrict ourselves to this specific set of approaches is for clarity of the paper and the ease by which these approaches can be applied. Other approaches not explored in the current study include a recently introduced statistical method to test the null-hypothesis that a sample of networks are generated by the same random process (Fujita et al., 2017), a multi-threshold permutation correction method (Drakesmith et al., 2015), a clustering optimisation approach (Smith et al., 2015), the union of shortest paths (Meier et al., 2015) and the minimally connected component (Jalili, 2016). The disadvantage of the latter is, however, that connectedness of the network is not guaranteed. In the current study, some of the explored approaches (ECO and MST) guarantee a fixed link density, which avoids biases due to differences in link density between groups. The union of shortest paths does, however, the exact opposite: A specific topological network is fixed, which allows one to detect for which density this topology emerges.

To conclude, similar to single layer networks, multilayer networks are also affected by non-topological biases of the network such as differences in link density and average connectivity. Whenever these biases are left uncorrected, this could lead to a risk of unreproducible results between centres and studies in a similar manner as for single layer networks. We therefore recommend using correction schemes prior to multilayer network analysis for group comparisons. Given the current explorations to correct for non-topological biases such as link density and average connectivity we recommend the following correcting approaches for multilayer networks: whenever a multilayer network consisting of networks obtained from different modalities is in question, one can apply either MST, ECO or SVD correction schemes to its individual layers. However, when treating a multilayer network where the layers correspond to complete networks obtained from the same modality and connectivity metric (based on the present analysis) SVD is a recommended approach. Future studies should explore the applicability of other existing approaches in the context of multilayer networks.

Acknowledgements

We thank the University of Nottingham for Vice Chancellor's Scholarship awarded to KM. This work was funded by a Medical Research Council New Investigator Research Grant (MR/M006301/1) awarded to

MJB. We also acknowledge Medical Research Council Partnership Grant (MR/K005464/1). Data used were collected as part of the University of Nottingham Multimodal Imaging Study in Psychosis, funded by the Medical Research Council (MR/J01186X/1). We therefore express our thanks to all those involved in data collection, particularly Emma Hall, Sian Robson and Jyothika Kumar.

References

Ashburner, J., Andersson, J.L.R., Friston, K.J., 1999. High-dimensional image registration using symmetric priors. Neuroimage 9, 619–628.

Bassett, D.S., Bullmore, E., Verchinski, B.A., Mattay, V.S., Weinberger, D.R., Meyer-Lindenberg, A., 2008. Hierarchical organization of human cortical networks in health and schizophrenia. J. Neurosci. 28, 9239–9248.

Bassett, D.S., Porter, M.A., Wymbs, N.F., Grafton, S.T., Carlson, J.M., Mucha, P.J., 2013. Robust detection of dynamic community structure in networks. Chaos an Interdiscip. J. Nonlinear Sci. 23, 13142.

Bassett, D.S., Sporns, O., 2017. Network neuroscience. Nat. Neurosci. 20, 353–364.

Bastos, A.M., Schoffelen, J.-M., 2015. A tutorial review of functional connectivity analysis methods and their interpretational pitfalls. Front. Syst. Neurosci. 9.

Battiston, F., Nicosia, V., Chavez, M., Latora, V., 2017. Multilayer motif analysis of brain networks. Chaos an Interdiscip. J. Nonlinear Sci. 27, 47404.

Battiston, F., Nicosia, V., Latora, V., 2014. Structural measures for multiplex networks. Phys. Rev. E 89, 32804.

Bazzi, M., Jeub, L.G.S., Arenas, A., Howison, S.D., Porter, M.A., 2016. Generative Benchmark Models for Mesoscale Structure in Multilayer Networks. arXiv Prepr. arXiv1608.06196.

Benson, A.R., Gleich, D.F., Leskovec, J., 2016. Higher-order organization of complex networks. Sci. (80-.) 353, 163–166.

Bentley, B., Branicky, R., Barnes, C.L., Chew, Y.L., Yemini, E., Bullmore, E.T., Vértes, P.E., Schafer, W.R., 2016. The multilayer connectome of Caenorhabditis elegans. PLoS Comput. Biol. 12, e1005283.

Boccaletti, S., Bianconi, G., Criado, R., Del Genio, C.I., Gómez-Gardenes, J., Romance, M., Sendina-Nadal, I., Wang, Z., Zanin, M., 2014. The structure and dynamics of multilayer networks. Phys. Rep. 544, 1–122.

Braun, U., Schäfer, A., Walter, H., Erk, S., Romanczuk-Seiferth, N., Haddad, L., Schweiger, J.I., Grimm, O., Heinz, A., Tost, H., 2015. Dynamic reconfiguration of frontal brain networks during executive cognition in humans. Proc. Natl. Acad. Sci. 112, 11678–11683.

Brookes, M.J., Hale, J.R., Zumer, J.M., Stevenson, C.M., Francis, S.T., Barnes, G.R., Owen, J.P., Morris, P.G., Nagarajan, S.S., 2011a. Measuring functional connectivity using MEG: methodology and comparison with fcMRI. Neuroimage 56, 1082–1104.

Brookes, M.J., Tewarie, P.K., Hunt, B.A.E., Robson, S.E., Gascoyne, L.E., Liddle, E.B., Liddle, P.F., Morris, P.G., 2016. A multi-layer network approach to MEG connectivity analysis. Neuroimage 132, 425–438.

Brookes, M.J., Woolrich, M., Luckhoo, H., Price, D., Hale, J.R., Stephenson, M.C., Barnes, G.R., Smith, S.M., Morris, P.G., 2011b. Investigating the electrophysiological basis of resting state networks using magnetoencephalography. Proc. Natl. Acad. Sci. 108, 16783–16788.

Buldú, J.M., Porter, M.A., 2017. Frequency-based Brain Networks: from a Multiplex Framework to a Full Multilayer Description. arXiv Prepr. arXiv1703.06091.

Colclough, G.L., Brookes, M.J., Smith, S.M., Woolrich, M.W., 2015. A symmetric multivariate leakage correction for MEG connectomes. Neuroimage 117, 439–448.

Colclough, G.L., Woolrich, M.W., Tewarie, P.K., Brookes, M.J., Quinn, A.J., Smith, S.M., 2016. How reliable are MEG resting-state connectivity metrics? Neuroimage 138, 284–293.

Crofts, J.J., Forrester, M., O'Dea, R.D., 2016. Structure-function clustering in multiplex brain networks. EPL Europhys. Lett. 116, 18003.

Crossley, N.A., Mechelli, A., Scott, J., Carletti, F., Fox, P.T., McGuire, P., Bullmore, E.T., 2014. The hubs of the human connectome are generally implicated in the anatomy of brain disorders. Brain 137, 2382–2395.

Crossley, N.A., Mechelli, A., Vértes, P.E., Winton-Brown, T.T., Patel, A.X., Ginestet, C.E., McGuire, P., Bullmore, E.T., 2013. Cognitive relevance of the community structure of the human brain functional coactivation network. Proc. Natl. Acad. Sci. 110, 11583–11588.

De Domenico, M., 2017. Multilayer modeling and analysis of human brain networks. Giga Sci. 6, 1–8.

De Domenico, M., Nicosia, V., Arenas, A., Latora, V., 2015a. Structural reducibility of multilayer networks. Nat. Commun. 6, 6864.

De Domenico, M., Sasai, S., Arenas, A., 2016. Mapping multiplex hubs in human functional brain networks. Front. Neurosci. 10.

De Domenico, M., Solé-Ribalta, A., Cozzo, E., Kivelä, M., Moreno, Y., Porter, M.A., Gómez, S., Arenas, A., 2013. Mathematical formulation of multilayer networks. Phys. Rev. X 3, 41022.

De Domenico, M., Solé-Ribalta, A., Omodei, E., Gómez, S., Arenas, A., 2015b. Ranking in interconnected multilayer networks reveals versatile nodes. Nat. Commun. 6.

De Moor, B., 1993. The singular value decomposition and long and short spaces of noisy matrices. IEEE Trans. Signal Process 41, 2826–2838.

Dijkstra, E.W., 1959. A note on two problems in connexion with graphs. Numer. Math. 1, 269–271.

Doesburg, S.M., Roggeveen, A.B., Kitajo, K., Ward, L.M., 2008. Large-scale gamma-band phase synchronization and selective attention. Cereb. Cortex 18, 386–396.

Drakesmith, M., Caeyenberghs, K., Dutt, A., Lewis, G., David, A.S., Jones, D.K., 2015. Overcoming the effects of false positives and threshold bias in graph theoretical analyses of neuroimaging data. Neuroimage 118, 313–333.

Ellens, W., Spieksma, F.M., Van Mieghem, P., Jamakovic, A., Kooij, R.E., 2011. Effective graph resistance. Linear Algebra Appl. 435, 2491–2506.

Fallani, F.D.V., Latora, V., Chavez, M., 2017. A topological criterion for filtering information in complex brain networks. PLoS Comput. Biol. 13, e1005305.

Fries, P., 2009. Neuronal gamma-band synchronization as a fundamental process in cortical computation. Annu. Rev. Neurosci. 32, 209–224.

Fujita, A., Vidal, M.C., Takahashi, D.Y., 2017. A statistical method to distinguish functional brain networks. Front. Neurosci. 11.

Garcés, P., Pereda, E., Hernández-Tamames, J.A., Del-Pozo, F., Maestú, F., Ángel Pineda-Pardo, J., 2016. Multimodal description of whole brain connectivity: a comparison of resting state MEG, fMRI, and DWI. Hum. Brain Mapp. 37, 20–34.

Golub, G.H., Van Loan, C.F., 2012. Matrix Computations. JHU Press.

Gomez, S., Diaz-Guilera, A., Gomez-Gardenes, J., Perez-Vicente, C.J., Moreno, Y., Arenas, A., 2013. Diffusion dynamics on multiplex networks. Phys. Rev. Lett. 110, 28701.

Gong, G., He, Y., Concha, L., Lebel, C., Gross, D.W., Evans, A.C., Beaulieu, C., 2009. Mapping anatomical connectivity patterns of human cerebral cortex using in vivo diffusion tensor imaging tractography. Cereb. Cortex 19, 524–536.

Goñi, J., van den Heuvel, M.P., Avena-Koenigsberger, A., de Mendizabal, N.V., Betzel, R.F., Griffa, A., Hagmann, P., Corominas-Murtra, B., Thiran, J.-P., Sporns, O., 2014. Resting-brain functional connectivity predicted by analytic measures of network communication. Proc. Natl. Acad. Sci. 111, 833–838.

Granell, C., Gómez, S., Arenas, A., 2013. Dynamical interplay between awareness and epidemic spreading in multiplex networks. Phys. Rev. Lett. 111, 128701.

Guillon, J., Attal, Y., Colliot, O., La Corte, V., Dubois, B., Schwartz, D., Chavez, M., Fallani, F.D.V., 2016. Loss of Inter-frequency Brain Hubs in Alzheimer's Disease. arXiv Prepr. arXiv1701.00096.

Halu, A., Mondragón, R.J., Panzarasa, P., Bianconi, G., 2013. Multiplex pagerank. PLoS One 8, e78293.

He, Y., Chen, Z.J., Evans, A.C., 2007. Small-world anatomical networks in the human brain revealed by cortical thickness from MRI. Cereb. Cortex 17, 2407–2419.

Hernández, J.M., Van Mieghem, P., 2011. Classification of Graph Metrics. Delft Univ. Technol. Tech. Rep.

Hernández, J.M., Wang, H., Van Mieghem, P., D'Agostino, G., 2014. Algebraic connectivity of interdependent networks. Phys. A Stat. Mech. its Appl. 404, 92–105.

Hillebrand, A., Barnes, G.R., Bosboom, J.L., Berendse, H.W., Stam, C.J., 2012. Frequency-dependent functional connectivity within resting-state networks: an atlas-based MEG beamformer solution. Neuroimage 59, 3909–3921.

Hincapié, A.-S., Kujala, J., Mattout, J., Pascarella, A., Daligault, S., Delpuech, C., Mery, D., Cosmelli, D., Jerbi, K., 2017. The impact of MEG source reconstruction method on source-space connectivity estimation: a comparison between minimum-norm solution and beamforming. Neuroimage 156, 29–42.

Hlinka, J., Coombes, S., 2012. Using computational models to relate structural and functional brain connectivity. Eur. J. Neurosci. 36, 2137–2145.

Huang, M.X., Mosher, J.C., Leahy, R.M., 1999. A sensor-weighted overlapping-sphere head model and exhaustive head model comparison for MEG. Phys. Med. Biol. 44, 423.

Hunt, B.A.E., Tewarie, P.K., Mougin, O.E., Geades, N., Jones, D.K., Singh, K.D., Morris, P.G., Gowland, P.A., Brookes, M.J., 2016. Relationships between cortical myeloarchitecture and electrophysiological networks. Proc. Natl. Acad. Sci. 113, 13510–13515.

Iacovacci, J., Rahmede, C., Arenas, A., Bianconi, G., 2016. Functional multiplex PageRank. EPL Europhys. Lett. 116, 28004.

Iturria-Medina, Y., Sotero, R.C., Canales-Rodríguez, E.J., Alemán-Gómez, Y., Melie-García, L., 2008. Studying the human brain anatomical network via diffusion-weighted MRI and Graph Theory. Neuroimage 40, 1064–1076.

Jalili, M., 2016. Functional brain networks: does the choice of dependency estimator and binarization method matter? Sci. Rep. 6.

Jensen, O., Tesche, C.D., 2002. Frontal theta activity in humans increases with memory load in a working memory task. Eur. J. Neurosci. 15, 1395–1399.

Karrer, B., Newman, M.E.J., 2011. Stochastic blockmodels and community structure in networks. Phys. Rev. E 83, 16107.

Kivelä, M., Arenas, A., Barthelemy, M., Gleeson, J.P., Moreno, Y., Porter, M.A., 2014. Multilayer networks. J. complex Netw. 2, 203–271.

Kruskal, J.B., 1956. On the shortest spanning subtree of a graph and the traveling salesman problem. Proc. Am. Math. Soc. 7, 48–50.

Larson-Prior, L.J., Oostenveld, R., Della Penna, S., Michalareas, G., Prior, F., Babajani-Feremi, A., Schoffelen, J.-M., Marzetti, L., de Pasquale, F., Di Pompeo, F., 2013. Adding dynamics to the human connectome project with MEG. Neuroimage 80, 190–201.

Lord, A., Ehrlich, S., Borchardt, V., Geisler, D., Seidel, M., Huber, S., Murr, J., Walter, M., 2016. Brain parcellation choice affects disease-related topology differences increasingly from global to local network levels. Psychiatry Res. Neuroimaging 249, 12–19.

Märtens, M., Meier, J., Hillebrand, A., Tewarie, P., Van Mieghem, P., 2017. Brain network clustering with information flow motifs. Appl. Netw. Sci. 2, 25.

Mehta-Pandejee, G., Robinson, P.A., Henderson, J.A., Aquino, K.M., Sarkar, S., 2017. Inference of direct and multistep effective connectivities from functional connectivity of the brain and of relationships to cortical geometry. J. Neurosci. Methods 283, 42–54.

Meier, J., Märtens, M., Hillebrand, A., Tewarie, P., Van Mieghem, P., 2016a. Motif-based analysis of effective connectivity in brain networks. In: International Workshop on Complex Networks and Their Applications. Springer, pp. 685–696.

Meier, J., Tewarie, P., Hillebrand, A., Douw, L., van Dijk, B.W., Stufflebeam, S.M., Van Mieghem, P., 2016b. A mapping between structural and functional brain networks. Brain Connect. 6, 298–311.
Meier, J., Tewarie, P., Van Mieghem, P., 2015. The union of shortest path trees of functional brain networks. Brain Connect. 5, 575–581.
Meunier, D., Lambiotte, R., Fornito, A., Ersche, K.D., Bullmore, E.T., 2010. Hierarchical modularity in human brain functional networks. Hierarchy Dyn. neural Netw. 1.
Micheloyannis, S., Pachou, E., Stam, C.J., Vourkas, M., Erimaki, S., Tsirka, V., 2006. Using graph theoretical analysis of multi channel EEG to evaluate the neural efficiency hypothesis. Neurosci. Lett. 402, 273–277.
Mucha, P.J., Richardson, T., Macon, K., Porter, M.A., Onnela, J.-P., 2010. Community structure in time-dependent, multiscale, and multiplex networks. Sci. (80-.) 328, 876–878.
Newman, M.E.J., 2006. Modularity and community structure in networks. Proc. Natl. Acad. Sci. 103, 8577–8582.
Nicosia, V., Bianconi, G., Latora, V., Barthelemy, M., 2014. Nonlinear growth and condensation in multiplex networks. Phys. Rev. E 90, 42807.
Nicosia, V., Bianconi, G., Latora, V., Barthelemy, M., 2013. Growing multiplex networks. Phys. Rev. Lett. 111, 58701.
Nicosia, V., Latora, V., 2015. Measuring and modeling correlations in multiplex networks. Phys. Rev. E 92, 32805.
Proix, T., Spiegler, A., Schirner, M., Rothmeier, S., Ritter, P., Jirsa, V.K., 2016. How do parcellation size and short-range connectivity affect dynamics in large-scale brain network models? Neuroimage 142, 135–149.
Robinson, P.A., 2012. Interrelating anatomical, effective, and functional brain connectivity using propagators and neural field theory. Phys. Rev. E 85, 11912.
Rubinov, M., Sporns, O., 2010. Complex network measures of brain connectivity: uses and interpretations. Neuroimage 52, 1059–1069.
Sahneh, F.D., Scoglio, C., 2014. Competitive epidemic spreading over arbitrary multilayer networks. Phys. Rev. E 89, 62817.
Sahneh, F.D., Scoglio, C., Van Mieghem, P., 2015. Exact coupling threshold for structural transition reveals diversified behaviors in interconnected networks. Phys. Rev. E 92, 40801.
Senkowski, D., Gallinat, J., 2015. Dysfunctional prefrontal gamma-band oscillations reflect working memory and other cognitive deficits in schizophrenia. Biol. Psychiatry 77, 1010–1019.
Smith, K., Azami, H., Parra, M.A., Starr, J.M., Escudero, J., 2015. Cluster-Span Threshold: an unbiased threshold for binarising weighted complete networks in functional connectivity analysis. In: Engineering in Medicine and Biology Society (EMBC), 2015 37th Annual International Conference of the IEEE. IEEE, pp. 2840–2843.
Smith, S.M., 2002. Fast robust automated brain extraction. Hum. Brain Mapp. 17, 143–155.
Smith, S.M., Jenkinson, M., Woolrich, M.W., Beckmann, C.F., Behrens, T.E.J., Johansen-Berg, H., Bannister, P.R., De Luca, M., Drobnjak, I., Flitney, D.E., 2004. Advances in functional and structural MR image analysis and implementation as FSL. Neuroimage 23, S208–S219.
Solá, L., Romance, M., Criado, R., Flores, J., García del Amo, A., Boccaletti, S., 2013. Eigenvector centrality of nodes in multiplex networks. Chaos an Interdiscip. J. Nonlinear Sci. 23, 33131.
Solé-Ribalta, A., De Domenico, M., Gómez, S., Arenas, A., 2014. Centrality rankings in multiplex networks. In: Proceedings of the 2014 ACM Conference on Web Science. ACM, pp. 149–155.
Stam, C.J., 2014. Modern network science of neurological disorders. Nat. Rev. Neurosci. 15, 683–695.
Stam, C.J., Jones, B.F., Nolte, G., Breakspear, M., Scheltens, P., 2007. Small-world networks and functional connectivity in Alzheimer's disease. Cereb. cortex 17, 92–99.
Stam, C.J., Tewarie, P., Van Dellen, E., Van Straaten, E.C.W., Hillebrand, A., Van Mieghem, P., 2014. The trees and the forest: characterization of complex brain networks with minimum spanning trees. Int. J. Psychophysiol. 92, 129–138.
Tewarie, P., Bright, M.G., Hillebrand, A., Robson, S.E., Gascoyne, L.E., Morris, P.G., Meier, J., Van Mieghem, P., Brookes, M.J., 2016a. Predicting haemodynamic networks using electrophysiology: the role of non-linear and cross-frequency interactions. Neuroimage 130, 273–292.
Tewarie, P., Hillebrand, A., van Dijk, B.W., Stam, C.J., O'Neill, G.C., Van Mieghem, P., Meier, J.M., Woolrich, M.W., Morris, P.G., Brookes, M.J., 2016b. Integrating cross-frequency and within band functional networks in resting-state MEG: a multi-layer network approach. Neuroimage 142, 324–336.
Tewarie, P., van Dellen, E., Hillebrand, A., Stam, C.J., 2015. The minimum spanning tree: an unbiased method for brain network analysis. Neuroimage 104, 177–188.
Tzourio-Mazoyer, N., Landeau, B., Papathanassiou, D., Crivello, F., Etard, O., Delcroix, N., Mazoyer, B., Joliot, M., 2002. Automated anatomical labeling of activations in SPM using a macroscopic anatomical parcellation of the MNI MRI single-subject brain. Neuroimage 15, 273–289.
van den Heuvel, M., de Lange, S., Zalesky, A., Seguin, C., Yeo, T., Schmidt, R., 2017. Proportional thresholding in resting-state fMRI functional connectivity networks and consequences for patient-control connectome studies: issues and recommendations. Neuroimage 152, 437–449.
Van Mieghem, P., 2016. Interconnectivity structure of a general interdependent network. Phys. Rev. E 93, 42305.
Van Mieghem, P., 2010. Graph Spectra for Complex Networks. Cambridge University Press.
Van Mieghem, P., Devriendt, K., Cetinay, H., 2017. Pseudo-inverse of the Laplacian and Best Spreader Node in a Network.
Van Wijk, B.C.M., Stam, C.J., Daffertshofer, A., 2010. Comparing brain networks of different size and connectivity density using graph theory. PLoS One 5, e13701.
Wang, H., Douw, L., Hernandez, J.M., Reijneveld, J.C., Stam, C.J., Van Mieghem, P., 2010. Effect of tumor resection on the characteristics of functional brain networks. Phys. Rev. E 82, 21924.
Wang, H., Li, Q., D'Agostino, G., Havlin, S., Stanley, H.E., Van Mieghem, P., 2013. Effect of the interconnected network structure on the epidemic threshold. Phys. Rev. E 88, 22801.
Wang, Z., Wang, L., Perc, M., 2014. Degree mixing in multilayer networks impedes the evolution of cooperation. Phys. Rev. E 89, 52813.
Wider, N., Garas, A., Scholtes, I., Schweitzer, F., 2016. Interconnected Networks, first ed. Springer https://doi.org/10.1007/978-3-319-23947-7.
Yu, M., Engels, M.M., Hillebrand, A., van Straaten, E.C., Gouw, A.A., Teunissen, C., van der Flier, W.M., Scheltens, P., Stam, C.J., 2017. Selective impairment of hippocampus and posterior hub areas in Alzheimer's disease: an MEG-based multiplex network study. Brain a J. Neurol. 140, 1466–1485.
Yu, M., Hillebrand, A., Tewarie, P., Meier, J., van Dijk, B., Van Mieghem, P., Stam, C.J., 2015. Hierarchical clustering in minimum spanning trees. Chaos an Interdiscip. J. Nonlinear Sci. 25, 23107.